Interseismic deformation at subduction zones investigated by 2D numerical modeling: insight on slab kinematic conditions
case study before the 2010 Maule earthquake

Marcelo Contreras, Muriel Gerbault , Andrés Tassara , Rodolfo Araya , Klaus Bataille

1- Geosciences Environnemnt Toulouse, CNRS UMR 5563, IRD U234, Obs. Midi-Pyrénées, Toulouse, France.
2- Dep[mtos] de Géologia y de Ingenieria Matematica, Facultad de Ciencias Fisicas y Matematicas, Universidad de Concepcion, Chile.

Summary

We study the interseismic deformation preceding the Mw8.8 2010 Maule earthquake, in order to gain insight into the fundamental factors controlling elastic strain build-up and release in subduction zones.
We first developed a linear elasticity solver to implement a realistic subducting plate geometry constrained by geophysical data. We tested the influence of plate thickness, up-and down-dip limits of the locked interplate zone, elastic parameters, and velocity reduction at the base of the subducted slab. Our modeled predictions compared with interseismic GPS observations across the Maule earthquake area, indicate a strong influence of the down-dip limit on surface deformation. However, the fit to observations is achieved only after reducing the velocity at the base of the subducted slab below the trench region to 10% of the far-field convergence rate.

We interpret this kinematic constrain with the help of complementary numerical models that gradually evolve toward longer time-scales and EVP rheology. We link this velocity reduction at the base of the subducting slab with its long-term high flexural stress above the mantle. Even a small amount of this high deviatoric stress may transfer towards the upper portion of the slab as strain energy that may participate into the mechanical loading of the megathrust, and therefore play a part in triggering large earthquakes.

The definition of initial and boundary conditions between short-term to long-term models evidence the mechanical inconsistencies that may appear when considering pre-flexed subducting slabs and unloaded underlying asthenosphere. This adresses the short-term and long term stress balance of the system and the storage of large stresses.

GPS interseismic data and fit with Slip Models

GPS-derived surface velocity vectors across the Arauco Peninsula (~37.3°S) in south Chile (topo/bathy map). Vectors calculated by Ruegg et al. (2009, blue dots) and Moreno et al. (2010, yellow dots) from measurements before the Mw8.8 2010 Maule earthquake. Contours of 3, 6 & 9 m of co-seismic slip of the 2010 event in red (Moreno et al., 2012).

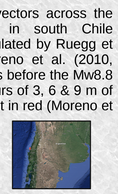

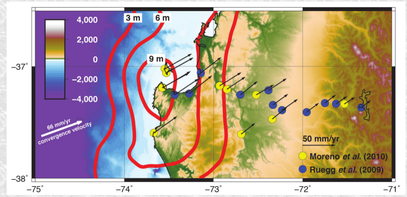

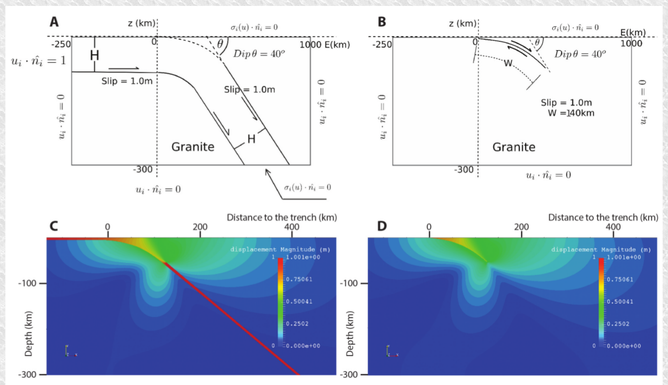

FIG. 3. Comparison of BSM and ESPM with thickness H=5 km. Panels **A** and **B** show the model setup for a ESPM and BSM respectively. Lower panels depicts the calculated displacement field after applying 1 m slip to the boundaries of the slab in a ESPM (**C**) and

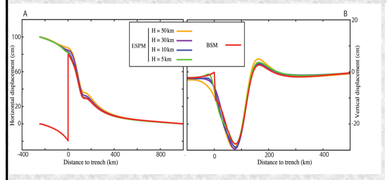

Comparison of horizontal (A) and vertical (B) surface displacement for BSM and ESPM with changing slab thickness H between 5 and 50 km.

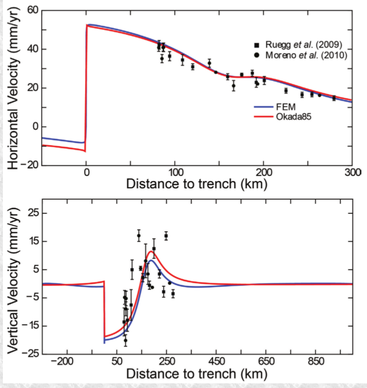

Modeled horizontal (A) and vertical (B) velocity and GPS observations with the analytical solution of Okada (1985) and our FEM solution reproducing the same BSM parameters used by Ruegg et al. (2009).

ESPM parametric study

ESPM approach in which the plate-mantle interface geometry is specifically designed for the Arauco peninsula (according to 3D geophysical data, Tassara and Echaurren, 2012).
Applied kinematic conditions at the plate and domain boundaries (note the tangential motion between plate and mantle, fraction of boundary velocity Ux).

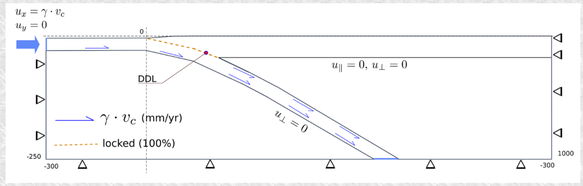

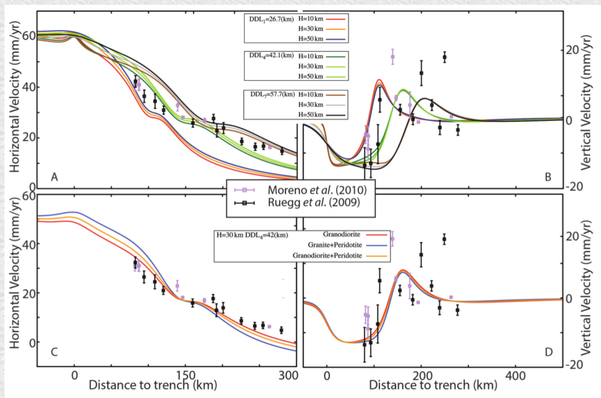

FIG. 7. ESPM Model results compared with GPS velocities along the Arauco Peninsula. Left-hand and right-hand panels show horizontal and vertical velocities respectively. With respect to uncertainties of GPS observations, surface displacement produced by the ESPM with realistic subduction geometry is almost insensitive to slab thickness H (as shown in **A** and **B**). Young Modulus E of the upper plate has a minor effect (as shown in **C** and **D**). Displacement is mostly controlled by the Downdip Limit (DDL) of interplate locking. Even our best fitting model (H=30 km, Granodiorite, DDL=42 km) is unable to reproduce the observed GPS velocities.

Necessity for Reduction in corner basal velocity

While Kanda et al.(2010) apply a velocity reduction at the basal corner of the slab due to its curvature, here we empirically increase this reducted velocity ($\mathcal{V}_{bcs}$), and seek for a best fit to the data.

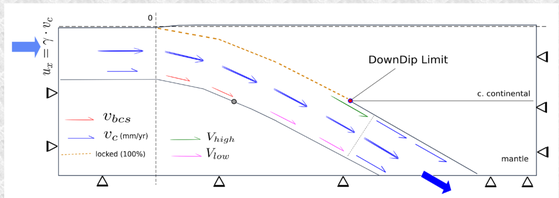

FIG. 8. Model setup for an ESPM with reduced velocity at the base of the slab due to bending. This is similar to figure 7 but here we introduce the possibility of reducing the displacement velocity at the base of the slab compared with the rest of plate as shown by arrows of different colors.

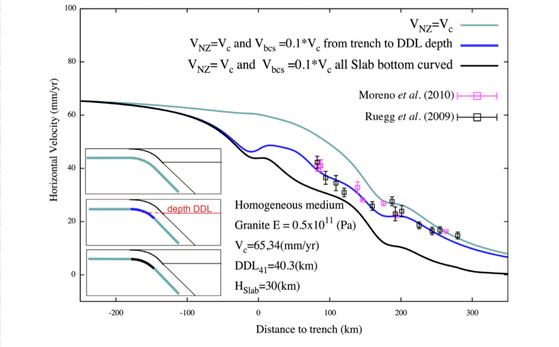

FIG. 9. Horizontal surface velocity resulting from a ESPM model that incorporates velocity reduction at the base of the slab. Our best ESPM notably improves the fitting to observed GPS rates if the velocity at the base of the slab is strongly reduced to 10% of the convergence velocity.

Lithosphere-mantle stress link, depend on boundary conditions

Three models set with code ADELI, in order to illustrate the mechanical interaction between the slab and the mantle.
Each three cases impose a tangential velocity along the base of the subducting plate, and no motion at the base of the overriding plate (as in the previous section). The deviatoric shear stresses that develop inside both plates reach ~100-200 MPa (turquoise to green), are equivalent in all three cases. However, all 3 cases assume different conditions for the underlying mantle:

A. Model AM-0 assumes that the mantle behaves as an inviscid fluid,

B. AM-1 includes a mantle with temperature dependent viscosity (of the order of 10^20 Pa.s): its lateral and bottom borders are set free-slip (similar to models in section 3).

C. AM-2 includes a temperature dependent mantle viscosity, but its boundaries react to Archimedes' restoring force (as if embedded in an infinite half space). The large stress field generated in the mantle results from the kinematic conditions applied the plate boundaries and in the mantle asthenosphere, thus illustrating how mechanical balance is achieved.

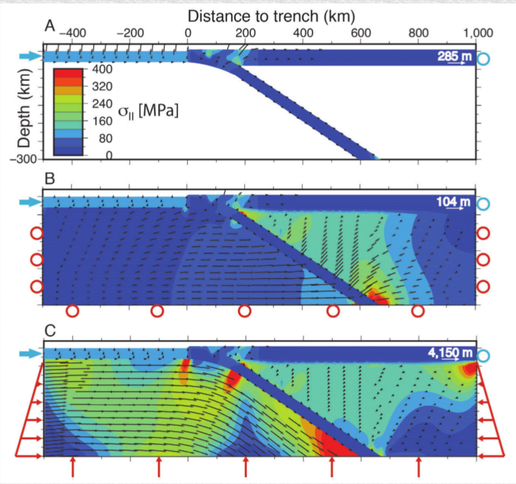

Long-term state of flexural stress

Stress distribution inside an elastic plate when considering long-term state of subduction, with applied velocities at plate boudaries, and Archimede's restoring force at asthenospheric depths; The lithosphere-asthenospheric system builds its 'quasi-static equilibrium".

A. Model AM-3, produced with code Adeli, with no gravity field, and with freely sliding plate-mantle boundaries (along which neither tangential nor normal motion are imposed). Within ~300 kyr of applied convergence from the right-hand side of the model (as in AM-2), flexural deviatoric stresses up to 260 MPa (in red) develop inside the elastic plate.

B. Model LM built with code Parovoz (modified from Gerbault et al., 2009 & Poliakov et al., 1993). Here gravity is included and the mantle and overriding plate both behave according to thermally dependent elasto-visco-plastic laws. Therefore their boundary is self-consistently defined and evolves throughout the time duration of the model. Within 4 Myr of applied far-field convergence, flexural stresses of the order of 1 GPa develop inside the elastic portion of the slab. Black and red lines display the orientation of principal tensile and compressional stress, respectively, typical of a flexural pattern.

C. Profiles along the base of the slab in case LM, determined by the isotherms around 600°C: accumulated shear strain (top), and shear stress (second invariant, bottom). At the slab's corner around X=-100 km stresses exceed 1 GPa, whereas the shear strain remains low (red rectangle domain). Such a stress concentration is equivalent to a frictional resistance that explains the need to reduce artificially the eastward velocity in this bend in the ESPM short-term kinematic approach.

We conclude that this concentration of high deviarotic stress may contribute in energy storage and seismic motion along the more deformable upper domains of the subduction zone.

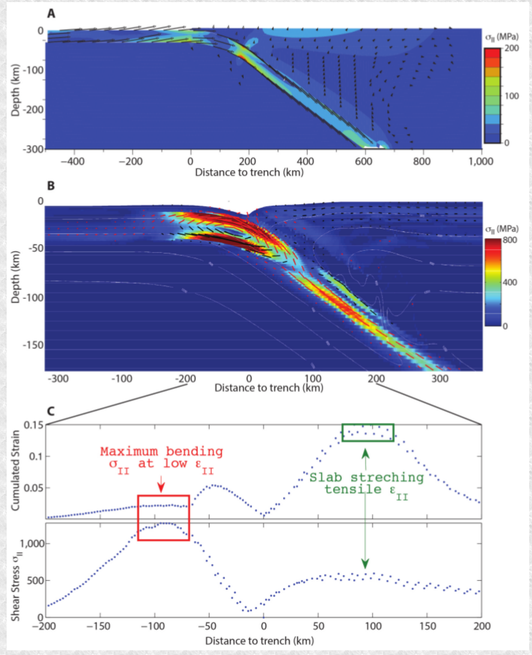

References:
Contreras, M., Tassara, A., Gerbault, M., Araya, R., & Bataille, K. (2016). Interseismic deformation at subduction zones investigated by 2D numerical modeling: case study before the 2010 Maule earthquake. *Andean Geology, 43(3)*, 247-262.
Hassani, R., Jongmans, D., Chéry, J. 1997. Study of plate deformation and stress in subduction processes using two-dimensional numerical models. J. *Geophys. Res. 102 (B8)*: 17951-17965.
Kanda, R.V.S.; Simons, M. 2010. An elastic plate model for interseismic deformation in subduction zones. J. *Geophys. Res. 115* (B3): B03405.
Moreno, M., Melnick, D., Rosenau, M., Baez, J., Klotz, J., Oncken, O., Tassara A., et al. (2012). Toward understanding tectonic control on the M w 8.8 2010 Maule Chile earthquake. *Earth Planet. Sci. Lett. 321*, 152-165.
Tassara, A., Echaurren, A. 2012. Anatomy of the Andean subduction zone: Three-dimensional density model upgraded and compared against global-scale models.Geophys. J. Int. 189: 161-168.